Preprint Title	First-principles study on elastic properties of Cu, $(Cu_{1-x}Ni_x)_3Sn$ and interfacial mechanical properties of $(Cu_{1-x}Ni_x)_3Sn$/Cu in the lead-free solder joint
Authors	Guomin Hua
Publication Date	06 Jan 2026
Article Type	Full Research Paper
ORCID® iDs	Guomin Hua - https://orcid.org/0000-0002-1564-4015

First-principles study on elastic properties of Cu, $(Cu_{1-x}Ni_x)_3Sn$ and interfacial mechanical properties of $(Cu_{1-x}Ni_x)_3Sn$/Cu in the lead-free solder joint

Guomin Hua[1]

[1] School of Material Science and Engineering, Jiangsu University, Zhenjiang 212013, Jiangsu, China

Abstract

In this study, the elastic properties of Cu and $(Cu_xNi_{1-x})_3Sn$ are calculated to reveal the effects of Ni alloying on the interfacial mechanical properties of $(Cu_xNi_{1-x})_3Sn$/Cu in lead-free solder joints. The results reveal that, within the thermodynamically stable domain of $(Cu_xNi_{1-x})_3Sn$, the increase of Ni content can enhance the interfacial mechanical properties of $(Cu_xNi_{1-x})_3Sn$/Cu, and increase the reliability of the lead-free solder joints. The enhancement mechanism can be attributed the improvements of orientated Young's modulus and ductility of $(Cu_xNi_{1-x})_3Sn$ achieved by Ni alloying. But higher Ni content beyond the thermodynamically stable domain of $(Cu_xNi_{1-x})_3Sn$ will deteriorate the interfacial mechanical properties by mechanical mechanism or thermodynamical mechanism, and decrease the reliability of the lead-free solder joints. The results presented in this study will not only unveil the effects of Ni alloying on the interfacial properties of lead-free solder joints, but also will provide a guidance for the high-performed lead-free solder design by alloying strategies to meet the requirements for electronic device miniaturization and harsh environmental applications.

key words: Lead-free Solder; Elastic Modulus; Ductility; work of adhesion; Interfacial Toughness;

[1] guomin@ujs.edu.cn

1.Introduction

Due to the toxicity of lead, it has caused serious problems in human health and environmental pollution, thus the use of lead-containing solder in electronic device packaging has been restricted by legislation[1]. In the last few decades, aiming to replace the lead-containing solders, great efforts have been dedicated to develop the lead-free solder with respect to the cost-effectiveness, wettability, melting point, corrosion resistances, mechanical and electrical properties[1,2]. A series of binary alloy solders, like Sn-Zn alloys[3], Sn-Cu alloys[4], Sn-Ag alloys[5], and Sn-Bi alloys[6], have been extensively investigated. Moreover, the ternary and quaternary alloys have recently received considerable attention, and the Sn-Ag-Cu ternary alloy is considered as the promising candidate to substitute the conventional lead-containing solder alloys[7].

Driven by the miniaturization of electronic devices and their widespread application in harsh environments such as high temperature and high humidity, the reliability of solder joints has become a major issue in practice[2,8]. As far as the lead-containing solder was concerned, the high quality of solder joints could be attributed to the formation of a continuous Pb layer, serving as a barrier layer to separate the intermetallics in solders from the substrate[9]. While, in contrast to the barrier layer formed in lead-containing soldering, the lead-free soldering formed a compact interface between the intermetallics and the substrate without a barrier layer[9]. The compact interface could result in poor resistance to high temperatures and thermal shocks. Therefore, high lead solder remains the preferred choice for high-temperature applications at present[1].

In view of the fact that Ni and Pb belong to the same group in the periodic table of elements, and have the similarly chemical and electronic properties[10], great interests have been intrigued to the enhance the reliability of lead-free solder joints by Ni alloying. For instance, Zhang et al. observed that the corrosion resistance of Sn-Zn solder can be enhanced by alloying of Ni, Cr, Cu and Ag, and the strengthened corrosion resistance follows the order as: Ag<Cu<Cr<Ni[11]. El-Taher et al. demonstrated the ductility and the strength of Sn–3.0Ag–0.5Cu lead-free solders could be enhanced by Ni alloying[12]. Although the beneficial effects of Ni alloying on the properties of lead-free solder have been demonstrated by these investigations, little attentions have been paid on the effects of Ni alloying on the interfacial mechanical properties of lead-free

solder joints.

Considering the important role of the interface between the intermetallics and the substrate played in the strength and reliability of solder joint, Gan et al. investigated the formation sequence of Cu_3Sn and Cu_6Sn_5 on the Cu substrate, and determined the orientation relationship of ε-Cu_3Sn/Cu interfaces as $(001)_\varepsilon // (111)_{Cu}$ and $[100]_\varepsilon // [\bar{1}10]_{Cu}$ [13], namely, the interface was constructed by attaching the (001) facet of ε-Cu_3Sn to the (111) facet of Cu substrate, at the same time, the $[100]$ axis of ε-Cu_3Sn paralleled to the $[\bar{1}10]$ axis of Cu substrate.

Therefore, according to the orientation relationship of the ε-Cu_3Sn/Cu interface, an attempt to reveal the effects of Ni alloying in the intermetallics on the strength and toughness of $(Cu_{1-x}Ni_x)_3Sn$/Cu interface has been made in this study. At first, the elastic properties of $(Cu_{1-x}Ni_x)_3Sn$ and Cu were calculated, followed by the intrinsic ductility evaluations in terms of elastic moduli. Subsequently, the orientation dependent Young's modulus of Cu and $(Cu_{1-x}Ni_x)_3Sn$ were calculated. Finally, the tensile modulus, ultimate tensile stress, work of adhesion and interfacial toughness of $(Cu_{1-x}Ni_x)_3Sn$ /Cu were calculated based the interface model with the orientation relationship of $(001)_\varepsilon // (111)_{Cu}$ and $[100]_\varepsilon // [\bar{1}10]_{Cu}$, and the underlying mechanisms responsible for the influence of Ni alloying on the work of adhesion and interfacial toughness were demonstrated.

2.Methodology

In this study, the first-principles calculations within the framework of density functional theory (DFT) were implemented by ABINIT package[14]. The norm-conserving pseudopotentials[15] and Perdew-Burke-Ernzerhof Generalized Gradient Approximation (GGA) of exchange-correlation functional[16] were adopted for the calculation. Regarding the calculations on the intetrmetallics,$(Cu_xNi_{1-x})_3Sn$, the virtual crystal approximations (VCA) were used to construct the virtual atoms standing for the mixture of Cu atoms and Ni atoms, namely, the pseudopotentials of the virtual atoms were constructed by $V_{CuNi}^{VCA}(\mathbf{r}) = xV_{Cu}(\mathbf{r}) + (1-x)V_{Ni}(\mathbf{r})$ [17]. As demonstrated by the previous

studies[18,19,20,21], the VCA could significantly enhance the calculation efficiency without losing the accuracy by reducing the model size of the alloying systems. Considering the phase stability of $(Cu_xNi_{1-x})_3Sn$[22], the content of Ni, 1-x, was set within the range for 0 at.% to 30 at.%. As far as the calculations of the structure optimizations and elastic properties were concerned, the kinetic energy cutoff of 30 Hartree, the k-point mesh of 8×8×8 and the potential residual V(r) of less than 10^{-8} Hartree were used to achieve self-consistent convergence.

Based on the optimized crystal structures, the elastic constants of cubic structured Cu and orthorhombic structured $(Cu_xNi_{1-x})_3Sn$ were calculated by the finite strain methods, where three deformations and nine deformations were built for Cu and $(Cu_xNi_{1-x})_3Sn$, respectively, due to three and nine independent elastic constants corresponding to cubic and orthorhombic crystals, respectively [23]. The strain magnitudes of -0.02, -0.01, 0.0, 0.01, 0.02 were used to calculated the energy increments of the deformed cells. By quadratic fitting the relation between the energy increments and the strains, the elastic constants of C_{11}, C_{12}, C_{44} for Cu and the elastic constants of C_{11}, C_{22}, C_{33}, C_{12}, C_{13}, C_{23}, C_{44}, C_{55}, C_{66} for $(Cu_xNi_{1-x})_3Sn$ were extracted. Based on the calculated elastic constants, the bulk modulus, shear modulus, Young's modulus, anisotropy and poisson ratio of Cu and $(Cu_xNi_{1-x})_3Sn$ were calculated According to Voight–Reuss–Hill bounds[24,25]. Furthermore, according to the calculated elastic constants, the orientation dependent Young's modulus of Cu and $(Cu_xNi_{1-x})_3Sn$ were calculated.

According to the orientation relationship of Cu_3Sn/Cu interfaces[13], i.e., $(001)_\varepsilon // (111)_{Cu}$ and $[100]_\varepsilon // [\bar{1}10]_{Cu}$, the interface was constructed by adhering the Cu slab and $(Cu_xNi_{1-x})_3Sn$ slab. The Cu slab consisted of four atomic layers, the $(Cu_xNi_{1-x})_3Sn$ slab consisted of three atomic layers, and the thickness of the vacuum layer was 1nm. The interfacial modulus, ultimate tensile stress, work of adhesion and the interfacial toughness of $(Cu_xNi_{1-x})_3Sn$ /Cu interfaces were determined by the tensile test along the direction normal to the interface plane, namely, along the z-axis. During the tensile deformation, the strain along the z-axis was fixed, at the same time, the stresses along the x-axis and y-axis were relaxed to less than 0.5GPa. For the calculations on the interface structure, the kinetic energy cutoff of 30 Hartree, the k-point mesh of 4×4×1 and the potential residual V(r) of less than 10^{-8} Hartree were used to achieve self-consistent convergence.

3.Results and Discussions

3.1 Elastic properties of Cu and $(Cu_xNi_{1-x})_3Sn$

Figure 1a presents the optimized crystal structures of Cu and $(Cu_xNi_{1-x})_3Sn$, where the Cu crystallizes into face-centered cubic (FCC) structure, and the $(Cu_xNi_{1-x})_3Sn$ crystallizes into orthorhombic structure. The Ni alloying in $(Cu_xNi_{1-x})_3Sn$ is represented by the virtual atoms that substitutes the Cu atoms in Cu_3Sn, the corresponding pseudopotentials of virtual atoms is constructed by virtual crystal approximation(VCA)[17]. Based on the optimized crystal structures, the elastic constants of Cu and $(Cu_xNi_{1-x})_3Sn$ are calculated by the finite strain methods. As listed in Table 1, the independent elastic constants of C_{11},C_{12} and C_{44} are 134.8, 109.5 and 51GPa, respectively, for FCC structured Cu. The calculated elastic constants of Cu are consistent with the measured elastic constants[26]. The independent elastic constants of C_{11}, C_{22}, C_{33}, C_{12}, C_{13}, C_{23}, C_{44}, C_{55} and C_{66} are 147.5, 165.0, 161.0, 82.9, 78.1, 79.4, 42.8, 47.4 and 45.5 GPa, respectively, for Cu_3Sn. The calculated elastic constants of Cu_3Sn are in good agreement with the reported elastic constants of Cu_3Sn by Pang et al.[27]. Furthermore, the dependence of the elastic constants of $(Cu_xNi_{1-x})_3Sn$ on the Ni content are presented in Figure 1b. It can be observed that pure tensile elastic constants, C_{11}, C_{22}, C_{33}, and orthogonal elastic constants, C_{12}, C_{13}, C_{23}, are significantly enhanced by the Ni alloying. While, only slight improvements of the pure shear elastic constants, C_{44}, C_{55}, C_{66}, are achieved by Ni alloying.

Based on the calculated elastic constants of Cu and $(Cu_xNi_{1-x})_3Sn$, the average bulk modulus, shear modulus, Young's modulus, universal anisotropy and Poisson ratio were calculated according to the Voigt-Reuss-Hill approximations[25]. For cubic structured Cu, the Voigt-type bulk modulus, B_V , shear modulus, G_V , and Reuss-type bulk modulus, B_R , shear modulus, G_R , can be calculated in terms of the elastic constants, C_{11}, C_{12} , C_{44}, as [25]:

$$\begin{aligned} B_V &= B_R = \left(C_{11} + 2C_{12}\right)/3 \\ G_V &= \left(C_{11} - C_{12} + 3C_{44}\right)/5 \\ G_R &= 5\left(C_{11} - C_{12}\right)C_{44} / \left[4C_{44} + 3\left(C_{11} - C_{12}\right)\right] \end{aligned} \quad (1)$$

For the orthorhombic structured $(Cu_xNi_{1-x})_3Sn$, the Voigt-type bulk modulus, B_V , shear modulus, G_V , and Reuss-type bulk modulus, B_R , shear modulus, G_R , can be calculated in terms

of the elastic constants, C_{11}, C_{22}, C_{33}, C_{12}, C_{13}, C_{23}, C_{44}, C_{55}, C_{66}, as[25]:

$$
\begin{aligned}
B_V &= (1/9)\left[C_{11}+C_{22}+C_{33}+2\left(C_{12}+C_{13}+C_{23}\right)\right] \\
B_R &= \Delta\left[\begin{array}{l} C_{11}\left(C_{22}+C_{33}-2C_{23}\right)+C_{22}\left(C_{33}-2C_{13}\right)-2C_{33}C_{12} \\ +C_{12}\left(2C_{23}-C_{12}\right)+C_{13}\left(2C_{12}-C_{13}\right)+C_{23}\left(2C_{13}-C_{23}\right)\end{array}\right]^{-1} \\
G_V &= (1/15)\left[C_{11}+C_{22}+C_{33}+3\left(C_{44}+C_{55}+C_{66}\right)-\left(C_{12}+C_{13}+C_{23}\right)\right] \\
G_R &= 15\left\{4\left[\begin{array}{l} C_{11}\left(C_{22}+C_{33}+C_{23}\right)+C_{22}\left(C_{33}+C_{13}\right) \\ +C_{33}C_{12}-C_{12}\left(C_{23}+C_{12}\right) \\ -C_{13}\left(C_{12}+C_{13}\right)-C_{23}\left(C_{13}+C_{23}\right)\end{array}\right]/\Delta+3\left[\begin{array}{l}\left(1/C_{44}\right)+\left(1/C_{55}\right) \\ +\left(1/C_{66}\right)\end{array}\right]\right\}^{-1}
\end{aligned}
\tag{2}
$$

where

$$
\Delta = C_{13}\left(C_{12}C_{23}-C_{13}C_{22}\right)+C_{23}\left(C_{12}C_{13}-C_{23}C_{11}\right)+C_{33}\left(C_{11}C_{22}-C_{12}^2\right)
$$

Then, the average bulk modulus B is calculated as the arithmetic average of B_V and B_R, i.e. $B=(1/2)\left(B_V+B_R\right)$. Likewise, the average shear modulus G, is calculated by $G=(1/2)\left(G_V+G_R\right)$. According to the bulk modulus B and shear modulus G, the Young's modulus E and Poisson ratio υ can be calculated as[25]:

$$
\begin{aligned}
E &= 9BG/\left(3B+G\right) \\
\upsilon &= \left(3B-2G\right)/\left[2\left(3B+G\right)\right]
\end{aligned}
\tag{3}
$$

The calculated bulk modulus, shear modulus, and Young's modulus of Cu and $(Cu_xNi_{1-x})_3Sn$ are presented in Figure 2a and listed in Table 2. As for Cu, the calculated bulk modulus of 117.9 GPa, shear modulus of 29.5 GPa, and Young's modulus of 81.8 GPa, are consistent with the experimental results[28]. Regarding the intermetallics $(Cu_xNi_{1-x})_3Sn$, the bulk modulus, shear modulus, and Young's modulus are greater than those of Cu, except that the bulk modulus of Cu_3Sn is less than that of Cu. At the same time, it can be observed that the bulk modulus, shear modulus, and Young's modulus of $(Cu_xNi_{1-x})_3Sn$ increase with the increase of Ni content.

Moreover, according to the calculated B_V, B_R, G_V and G_R, an universal anisotropy index A^U, developed by Ostoja-Starzewski et al., can be expressed as[29]:

$$
A^U = 5\frac{G_V}{G_R}+\frac{B_V}{B_R}-6 \tag{4}
$$

Owing to the fact that the mechanical response of crystals to the external loading is strongly

dependent on the elastic anisotropy, the anisotropy of Cu and $(Cu_xNi_{1-x})_3Sn$ are evaluated by the universal anisotropy index A^U , which is calculated by Equation 4. In general, the locally isotropic crystal possess the A^U of zero. As the elastic anisotropy of the crystal increases, the value of A^U will increases correspondingly. As shown in Figure 2b, the A^U of Cu is 2.77. It indicates that Cu is intrinsically anisotropic, although Cu is a cubic structured metal. In contrast to the anisotropy of Cu, the A^U of the orthorhombic structured Cu_3Sn is 0.052. This evidence implies that the Cu_3Sn is locally elastic isotropic. By Ni alloying, the A^U of $(Cu_{0.9}Ni_{0.1})_3Sn$ increases to 0.16. With a further increase of Ni content, the A^U of $(Cu_xNi_{1-x})_3Sn$ decreases from 0.121 in $(Cu_{0.8}Ni_{0.2})_3Sn$ to 0.107 in $(Cu_{0.7}Ni_{0.3})_3Sn$. These evidences demonstrate that orthorhombic structured $(Cu_xNi_{1-x})_3Sn$ are more isotropic than the cubic structured Cu.

Besides the elastic modulus and the anisotropy, the intrinsic ductility of Cu and $(Cu_xNi_{1-x})_3Sn$ is evaluated by the parameters of Poisson ratio υ and the ratio of bulk modulus to shear modulus (B/G). In principle, Poisson ratio is defined as the ratio of the transverse strain to the longitudinal strain, and it characterizes the resistance of materials to the distortion under mechanical loading[30]. In terms of Poisson ratio, the boundary of ductile to brittle transition (DTB) can be identified as $\upsilon = 0.31$[30]. As presented in Figure 2c, the calculated Poisson ratio of Cu is 0.384, which is in good agreement with the experimental value of 0.364[28]. It reveals that Cu is a kind of intrinsic ductile metals. For Cu_3Sn, the calculated Poisson ratio is 0.323, which locates in the vicinity of DTB boundary. This evidence indicates that the intrinsic ductility of Cu_3Sn is poor. However, by Ni alloying, the Poisson ratio of $(Cu_{0.9}Ni_{0.1})_3Sn$ increases up to 0.339. With further increase of Ni content, Poisson ratio of $(Cu_xNi_{1-x})_3Sn$ decrease slightly from 0.339 in $(Cu_{0.8}Ni_{0.2})_3Sn$ to 0.338 in $(Cu_{0.7}Ni_{0.3})_3Sn$.

In addition to Poisson ratio, another ductility index, i.e. the ratio of bulk modulus to shear modulus B/G, are adopted to evaluate the ductility of Cu and $(Cu_xNi_{1-x})_3Sn$. Due to the fact that the index B/G is a measure of the plastic flow at the crack tip, the low B/G will lead to a difficulty of the plastic flow and correspondingly result in a brittle behavior. In contrast, the high B/G will give rise to a ease of the plastic flow and result in a ductile behavior[31]. In terms of B/G, the boundary of DTB can be identified as $B/G = 2.4$[30]. As presented in Figure 2d, the B/G of Cu

is 4.0, which is obviously higher than the DTB boundary of 2.4. It indicates the intrinsic ductility of Cu. While, the B/G of Cu_3Sn is 2.49, which is close to the DTB boundary of 2.4. It manifests the poor ductility of Cu_3Sn. As the Ni alloying in Cu_3Sn, the B/G of $(Cu_{0.9}Ni_{0.1})_3Sn$ increases to 2.78. With the further increase of Ni content, the B/G of $(Cu_xNi_{1-x})_3Sn$ slightly decreases from 2.78 in $(Cu_{0.8}Ni_{0.2})_3Sn$ to 2.76 in $(Cu_{0.7}Ni_{0.3})_3Sn$. Overall, the ductility evaluations of Cu and $(Cu_xNi_{1-x})_3Sn$, in terms of Poisson ratio and B/G, are mutually consistent with each other.

From the Poisson ratio and B/G, it can be observed that the ductility of $(Cu_xNi_{1-x})_3Sn$ can be enhanced by Ni alloying, but the enhancement will be attenuated by high Ni content. The observed effect of Ni alloying on the ductility of $(Cu_xNi_{1-x})_3Sn$ seems to be consistent with the experimental observation that Ni alloying with low content could enhance the ductility of η-$(Cu,Ni)_6Sn_5$ intermetallic compound, but the mechanical performance would be deteriorated by high Ni content[12]. Herein, the reason why the high Ni content will leads to the decrease in Poisson ratio and B/G may be attributed to the fact that high Ni content will result in a structural instability[22].

3.2 orientation dependent Young's moduli of Cu and $(Cu_xNi_{1-x})_3Sn$

Considering the critical roles of orientation dependent elastic properties played in the mechanical properties of interfaces[19], the orientation dependent Young's modulus of Cu and $(Cu_xNi_{1-x})_3Sn$ were investigated. Regarding the cubic structured Cu, the orientation dependent Young's modulus E_{hkl}^{cubic} along the direction $\langle hkl \rangle$ is calculated as[32]:

$$\frac{1}{E_{hkl}^{cubic}} = s_{11} - 2\left[\left(s_{11} - s_{12}\right) - \frac{1}{2}s_{44}\right]\left(l_1^2 l_2^2 + l_2^2 l_3^2 + l_1^2 l_3^2\right) \tag{5}$$

Meanwhile, as for the orthorhombic structured $(Cu_xNi_{1-x})_3Sn$, the orientation dependent Young's modulus $E_{hkl}^{\text{orthorhombic}}$ along the direction $\langle hkl \rangle$ is calculated as[32]:

$$\begin{aligned}\frac{1}{E_{hkl}^{\text{orthorhombic}}} = {} & l_1^4 s_{11} + l_2^4 s_{22} + l_3^4 s_{33} + 2l_1^2 l_2^2 s_{12} + 2l_1^2 l_3^2 s_{13} + 2l_2^2 l_3^2 s_{23} \\ & + l_2^2 l_3^2 s_{44} + l_1^2 l_3^2 s_{55} + l_1^2 l_2^2 s_{66}\end{aligned} \tag{6}$$

where s_{11}, s_{22}, s_{33}, s_{12}, s_{13}, s_{23}, s_{44}, s_{55} and s_{66} are the elements of the elastic compliance matrix. The elastic compliance matrix is the inverse of the elastic constant matrix. l_1, l_2 and l_3

are the direction cosine of the $\langle hkl \rangle$ axis.

According to the elastic compliance matrix, i.e. the inverse of calculated elastic constant matrix, the 3-dimensional (3D) orientated Young's modulus of Cu and $(Cu_xNi_{1-x})_3Sn$ are calculated by Equation 5 and Equation 6, respectively. The maximum and minimum of Young's modulus and corresponding orientations are listed in Table 2. As shown in Figure 3a, the orientation dependent Young's modulus of cubic structured Cu exhibits a star-shaped surface, and the maximum Young's modulus is oriented along the body-diagonal direction, i.e. $\langle 111 \rangle$ direction. Whereas, as shown in Figure 3b-3e, the orientation dependent Young's moduli of $(Cu_xNi_{1-x})_3Sn$ exhibit sphere-shaped surface. By Ni alloying, the sphere-shaped surfaces of $(Cu_xNi_{1-x})_3Sn$ are stretched along the z-axis. As the Ni content increases, the direction of the maximum Young's modulus changes from off the z-axis in Cu_3Sn to along the z-axis in $(Cu_{0.9}Ni_{0.1})_3Sn$, $(Cu_{0.8}Ni_{0.2})_3Sn$ and $(Cu_{0.7}Ni_{0.3})_3Sn$. The shapes of the 3D orientated Young's moduli demonstrate that the anisotropy of cubic structured Cu is higher than those of orthorhombic structured $(Cu_xNi_{1-x})_3Sn$. The anisotropy of Cu and $(Cu_xNi_{1-x})_3Sn$ revealed by the 3D orientation dependent Young's modulus is consistent with the anisotropy measured by the universal anisotropy A^U .

By cutting the 3D orientated Young's moduli along the solid lines shown in Figure 3a-3e, the specific magnitude and direction of maximum Young's modulus of Cu and $(Cu_xNi_{1-x})_3Sn$ are analyzed by the 2-dimensional (2D) slice of (110) plane. The 2D Young's modulus for Cu is shown in Figure 3f. It can be seen that orientation dependent Young's modulus of Cu shows a 4-fold petal shaped profile, the maximum Young's modulus of 134.8 GPa is along the $\langle 111 \rangle$ direction. As shown in Figure 3g, the maximum Young's modulus of Cu_3Sn is 118.6 GPa with the orientation close to the $\langle 111 \rangle$ direction. As shown in Figure 3h-3j, the maximum Young's moduli of $(Cu_{0.9}Ni_{0.1})_3Sn$, $(Cu_{0.8}Ni_{0.2})_3Sn$ and $(Cu_{0.7}Ni_{0.3})_3Sn$ are147.9, 161.8 and 177.8 GPa, respectively, with the orientation close to $\langle 001 \rangle$ direction. These results reveal that the Ni alloying in $(Cu_xNi_{1-x})_3Sn$ will not only increases the magnitude of the maximum Young's modulus, but also turns the orientation of the maximum Young's modulus from off z-axis direction to along z-axis direction.

3.3 Interfacial mechanical properties of $(Cu_xNi_{1-x})_3Sn/Cu$

In the following, the mechanical properties of $(Cu_xNi_{1-x})_3Sn/Cu$ interfaces were investigated. As shown in Figure 4a, the interface structure of $(Cu_xNi_{1-x})_3Sn/Cu$ consisted of a $(Cu_xNi_{1-x})_3Sn$ slab with 3 atomic layers, a Cu slab with 4 atomic layers and a vacuum layer with thickness of 1 nm. The adjacent atomic layers of Cu slab and $(Cu_xNi_{1-x})_3Sn$ slab are free, and the rest atomic layers of Cu slab and $(Cu_xNi_{1-x})_3Sn$ slab are fixed. The thickness of the interface layer is defined as thickness of free atomic layers, *a*. As the tensile stress applied along the direction normal to the interface plane, the relationship between the tensile stress and tensile strain of $(Cu_xNi_{1-x})_3Sn/Cu$ interfaces are calculated, as shown in Figure 4b. From the tensile stress-tensile strain curves, the tensile modulus($E_{tensile}$) are determined by the ratio of the tensile stress to the corresponding tensile strain, where the tensile strain is within the range from 0.00 to 0.03. As shown in Figure 4c, the tensile moduli of $(Cu_xNi_{1-x})_3Sn/Cu$ interfaces increase from 60.3 GPa in Cu_3Sn/Cu to 76.7 GPa in $(Cu_{0.7}Ni_{0.3})_3Sn/Cu$. The increase of the tensile modulus can be attributed to the fact that the Young's moduli of $(Cu_xNi_{1-x})_3Sn$ along $\langle 001 \rangle$ direction increase with the Ni content.

Furthermore, according to the tensile stress-tensile strain curves, the ultimate tensile strength (UTS) and corresponding tensile strain are determined, where the UTS is corresponding the maximum tensile stress that the interface structures can endure. As shown in Figure 4d, the UTS of $(Cu_xNi_{1-x})_3Sn/Cu$ interfaces increase from 4.35 GPa in Cu_3Sn/Cu to 5.13 GPa in $(Cu_{0.7}Ni_{0.3})_3Sn/Cu$. The tensile strain corresponding to UTS of $(Cu_xNi_{1-x})_3Sn/Cu$ interfaces increase from the 0.16 in Cu_3Sn/Cu to 0.19 in $(Cu_{0.8}Ni_{0.2})_3Sn/Cu$. However, with the further increase of Ni content, the tensile strain corresponding to UTS of $(Cu_{0.7}Ni_{0.3})_3Sn/Cu$ decreases to 0.13.

As far as the interfacial stability is concerned, it is generally characterized by the work of adhesion, i.e., the work required to separate the interface structure into two parts[33]. Due to the UTS corresponding to the maximum stress that the interface structure can endure, in other words, UTS is corresponding to the initiation of the interface structure destabilization, thus, the bulk energy density stored in the interface structure can be calculated by integrating the product of tensile stress and tensile strain on the tensile strain from 0 to strain at UTS. Then, the work of adhesion can be calculated by the product of the bulk energy density and thickness of the

interface layer, namely, the areal energy density stored during the tensile stretch before the structure destabilization reached. Therefore, the work of adhesion W_{ad} can be expressed as[19]:

$$W_{ad}=a\times\int_{0}^{\text{strain at UTS}}\sigma\times\varepsilon d\varepsilon \quad (7)$$

where a is the thickness of the interface layer in unit of m; σ is the tensile stress in unit of Pa; ε is the tensile strain, a dimensionless quantity. As shown in Figure 4e, the calculated W_{ad} of Cu_3Sn/Cu, $(Cu_{0.9}Ni_{0.1})_3Sn$/Cu, $(Cu_{0.8}Ni_{0.2})_3Sn$/Cu and $(Cu_{0.7}Ni_{0.3})_3Sn$/Cu are 0.349, 0.374, 0.483, 0.305 J/m^2, respectively. The maximum W_{ad} of 0.483 J/m^2 is achieved in $(Cu_{0.8}Ni_{0.2})_3Sn$/Cu, it can be attributed to the high UTS and large tensile strain at UTS.

According to the calculated work of adhesion W_{ad} and tensile modulus $E_{tensile}$, the interfacial toughness of $(Cu_xNi_{1-x})_3Sn$/Cu can be calculated as follows[33]:

$$K_{\text{IC}}^{\text{interface}}=\sqrt{4W_{ad}E_{tensile}}/10^6 \quad (8)$$

where $K_{\text{IC}}^{\text{interface}}$ is the interfacial toughness in unit of MPa·m$^{0.5}$, W_{ad} is in unit of J/m^2, $E_{tensile}$ is in unit of Pa. As presented in Figure 4f and listed in Table 3, the calculated interfacial toughness of Cu_3Sn/Cu, $(Cu_{0.9}Ni_{0.1})_3Sn$/Cu, $(Cu_{0.8}Ni_{0.2})_3Sn$/Cu and $(Cu_{0.7}Ni_{0.3})_3Sn$/Cu are 0.290, 0.325, 0.377, 0.306 MPa·m$^{0.5}$,respectively. It can be seen that the interfacial toughness of $(Cu_xNi_{1-x})_3Sn$/Cu increases with the increase of Ni content, as the composition changes from Cu_3Sn/Cu to $(Cu_{0.8}Ni_{0.2})_3Sn$/Cu. But further increase of Ni content, the interfacial toughness will be deteriorated as indicated by the fact that the interfacial toughness of $(Cu_{0.7}Ni_{0.3})_3Sn$/Cu decrease to 0.306 MPa·m$^{0.5}$.

As for the mechanism responsible for the effects of Ni alloying on the interfacial mechanical properties of $(Cu_xNi_{1-x})_3Sn$/Cu, the interfacial toughness increases with the Ni content, as the composition changes from Cu_3Sn/Cu to $(Cu_{0.8}Ni_{0.2})_3Sn$/Cu. Such improvement can be related to the enhanced orientated Young's modulus and ductility of $(Cu_xNi_{1-x})_3Sn$. The orientation Young's modulus of $(Cu_xNi_{1-x})_3Sn$, along $\langle 001\rangle$ direction, increases from 109.0 GPa in Cu_3Sn to 161.8 GPa in $(Cu_{0.8}Ni_{0.2})_3Sn$. At the same time, the ductility of $(Cu_xNi_{1-x})_3Sn$, in terms of B/G index, increases from 2.49 in Cu_3Sn to 2.78 in $(Cu_{0.8}Ni_{0.2})_3Sn$. Owing to the enhanced orientated Young's

modulus and ductility, both of UTS and tensile strain at UTS increase as the composition changes from Cu_3Sn/Cu to $(Cu_{0.8}Ni_{0.2})_3Sn$/Cu. The enhanced UTS and tensile strain at UTS will lead to an improvement of the work of adhesion, and in turn result in a reinforced interfacial toughness.

As for the deterioration of the interfacial toughness of $(Cu_{0.7}Ni_{0.3})_3Sn$/Cu with high Ni content, it can be attributed to the higher orientated Young's modulus and attenuated ductility. Because the oriented Young's modulus of $(Cu_{0.7}Ni_{0.3})_3Sn$ increases up to 177.8 GPa, and the ductility decreases to 2.76, The higher UTS will result in the premature destabilization in interface layer, and shortened the tensile strain at UTS. Although the UTS increases, the shortened tensile strain at UTS severely reduces the work of adhesion, and in turn decreases the interfacial toughness. In view of $(Cu_xNi_{1-x})_3Sn$ that is thermodynamically stabilized within the range from x=1 to x=0.72[22], another factor that causes the deterioration of the interfacial toughness of $(Cu_{0.7}Ni_{0.3})_3Sn$/Cu may be the stability of $(Cu_{0.7}Ni_{0.3})_3Sn$ in thermodynamics.

Overall, within the thermodynamically stable domain of $(Cu_xNi_{1-x})_3Sn$, the interfacial toughness of $(Cu_xNi_{1-x})_3Sn$/Cu increases with the increase of Ni content, it is dominated by the mechanical mechanism. While, for the case of high Ni content, the deterioration of the interfacial toughness may be caused by the mechanical mechanism or thermodynamic mechanism.

Conclusions

In summary, firstly, the calculated elastic properties of Cu and $(Cu_xNi_{1-x})_3Sn$ reveal that the Ni alloying in $(Cu_xNi_{1-x})_3Sn$ can effectively improve the pure tensile elastic constants and orthogonal elastic constants, but slightly improve the pure shear elastic constants. The improvement on elastic constants made by Ni alloying can result in the improvement of elastic modulus and ductility of $(Cu_xNi_{1-x})_3Sn$ with the increase of Ni content. However, under the condition of high Ni content, the improvement on the ductility made by Ni alloying will be attenuated.

Secondly, the calculated orientated Young's modulus of Cu and $(Cu_xNi_{1-x})_3Sn$ reveal that anisotropy of cubic structured Cu is higher than those of orthorhombic structured $(Cu_xNi_{1-x})_3Sn$. The maximum Young's modulus of Cu is orientated along the $\langle 111 \rangle$ direction. However, with the increase of Ni content, the orientation of the maximum Young's modulus of $(Cu_xNi_{1-x})_3Sn$ changes from $\langle 111 \rangle$ direction of Cu_3Sn to $\langle 001 \rangle$ direction of $(Cu_{0.7}Ni_{0.3})_3Sn$.

Finally, according to the orientation relationship of $(Cu_xNi_{1-x})_3Sn/Cu$ interface, the calculated tensile stress Vs. tensile strain curves of $(Cu_xNi_{1-x})_3Sn/Cu$ interfaces reveal that the tensile moduli and UTS monotonically increase with the increase of Ni content. Whereas, the work of adhesion and interfacial toughness increase with the increase of Ni content within the thermodynamically stable domain of $(Cu_xNi_{1-x})_3Sn$, the mechanism responsible for the enhancement of interfacial mechanical properties can be attributed the improvements of orientated Young's modulus and ductility of $(Cu_xNi_{1-x})_3Sn$ achieved by Ni alloying. With the further increase of Ni content beyond the thermodynamically stable domain, the work of adhesion and interfacial toughness of $(Cu_xNi_{1-x})_3Sn/Cu$ interfaces will be deteriorated. Such deterioration made by high Ni content can be attributed to the premature destabilization of the interface structure owing to the higher orientation Young's modulus and attenuated ductility of $(Cu_xNi_{1-x})_3Sn$. In addition, the thermodynamically instability of $(Cu_xNi_{1-x})_3Sn$ may also deteriorate the work of adhesion and interfacial toughness.

Overall, within the thermodynamically stable domain of $(Cu_xNi_{1-x})_3Sn$, the increase of Ni content can enhance the interfacial mechanical properties of $(Cu_xNi_{1-x})_3Sn/Cu$, and increase the reliability of the lead-free solder joints. But higher Ni content beyond the thermodynamically stable domain of $(Cu_xNi_{1-x})_3Sn$ will deteriorate the interfacial mechanical properties by mechanical mechanism or thermodynamical mechanism, and decrease the reliability of the lead-free solder joints.

Acknowledgement

In this study, the atomic models depicted in the graphical abstract were plotted by VESTA [34].

CRediT Author contributions

Guomin Hua: Conceptualization, Methodology, Investigation, Visualization, Writing – original draft, Writing – review & editing.

Declaration of Conflicts of interest

There are no conflicts of interest to declare and no known competing financial interests or personal relationships that could have appeared to influence the work reported in this article.

Data Availability Statement

The authors confirm that the data supporting the findings of this study are available within the article.

Figure Captions

Figure 1: (a) the crystal structures of Cu and $(Cu_xNi_{1-x})_3Sn$, where the virtual crystal approximation (VCA) is adopted for $(Cu_xNi_{1-x})_3Sn$ and the atomic models were plotted by VESTA[34]. This content is not subject to CC BY 4.0.; (b) the independent elastic constants, c_{11},c_{22}, c_{33}, c_{12}, c_{13}, c_{23}, c_{44}, c_{55}, c_{66}, of $(Cu_xNi_{1-x})_3Sn$ and the independent elastic constants, c_{11}, c_{12}, c_{44}, of Cu.

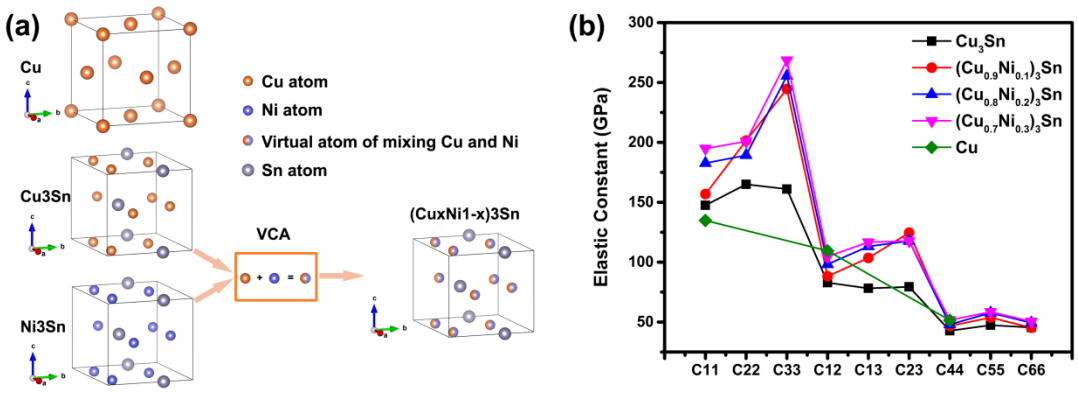

Figure 2: (a) The Bulk moduli, Shear moduli and Young's moduli of Cu and $(Cu_xNi_{1-x})_3Sn$; (b) Universal anisotropy of Cu and $(Cu_xNi_{1-x})_3Sn$; (c) Poisson ratios of Cu and $(Cu_xNi_{1-x})_3Sn$; (d) the ratio of bulk moduli to shear moduli, B/G, of Cu and $(Cu_xNi_{1-x})_3Sn$; The green horizontal lines in (c) and (d) correspond to the boundaries of the ductile to brittle transition.

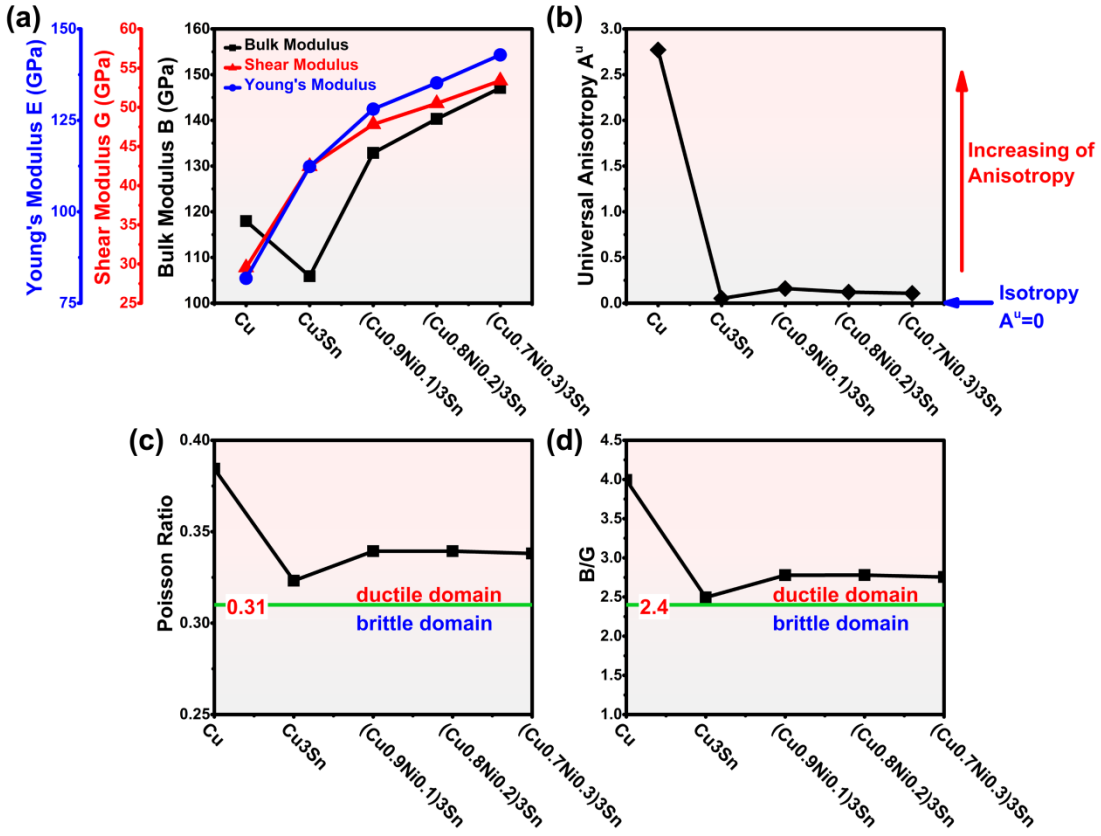

Figure 3: The three-dimensional (3D) surfaces of orientated Young's moduli for (a) Cu, (b) Cu_3Sn, (c) $(Cu_{0.9}Ni_{0.1})_3Sn$, (d) $(Cu_{0.8}Ni_{0.2})_3Sn$, (e) $(Cu_{0.7}Ni_{0.3})_3Sn$; the two-dimensional (2D) profiles on (110) plane of orientated Young's moduli for (f) Cu, (g) Cu_3Sn, (h) $(Cu_{0.9}Ni_{0.1})_3Sn$, (i) $(Cu_{0.8}Ni_{0.2})_3Sn$, (j) $(Cu_{0.7}Ni_{0.3})_3Sn$; the orientations of the maximum Young's moduli in the 2D profiles are denoted by the red lines.

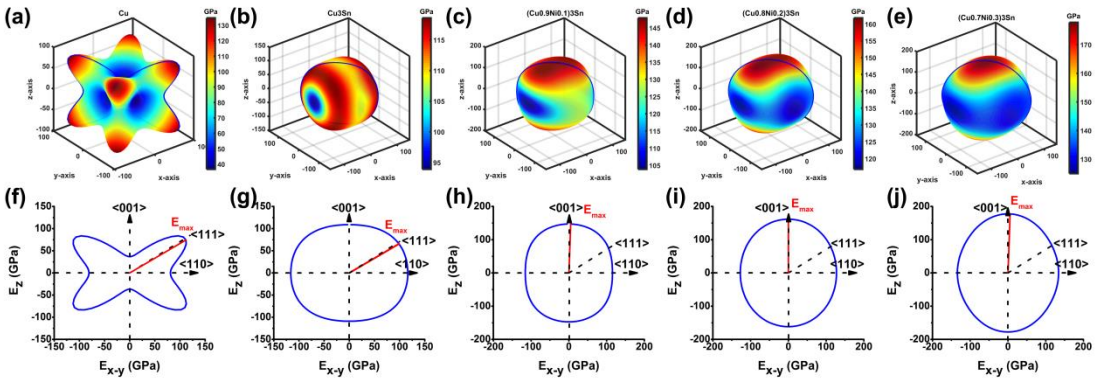

Figure 4: (a) the orientation relationship and structure of $(Cu_xNi_{1-x})_3Sn/Cu$ interfaces, and the atomic models were plotted by VESTA[34]. This content is not subject to CC BY 4.0.; (b) the tensile stress Vs. tensile strain curves of $(Cu_xNi_{1-x})_3Sn/Cu$ interfaces; (c) the tensile moduli, $E_{tensile}$, of $(Cu_xNi_{1-x})_3Sn/Cu$ interfaces; (d) the ultimate tensile stresses, UTS, and the tensile strains at UTS of $(Cu_xNi_{1-x})_3Sn/Cu$ interfaces; (e) the work of adhesion of $(Cu_xNi_{1-x})_3Sn/Cu$ interfaces; (f) the interfacial toughness of $(Cu_xNi_{1-x})_3Sn/Cu$ interfaces.

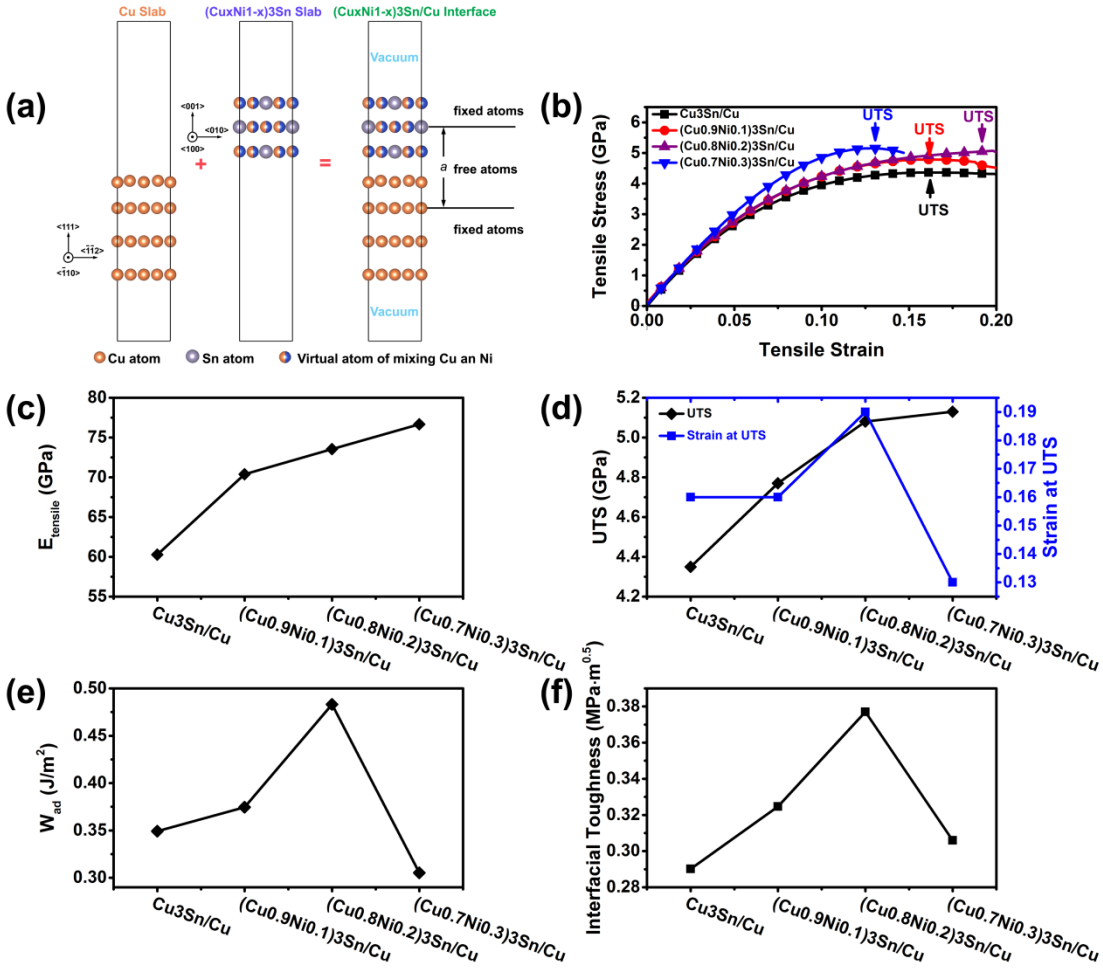

Tables

Table 1: Independent elastic constants of C_{11}, C_{12}, C_{44} for cubic structured Cu; Independent elastic constants of C_{11}, C_{22}, C_{33}, C_{12}, C_{13}, C_{23}, C_{44}, C_{55}, C_{66} for orthorhombic structured $(Cu_xNi_{1-x})_3Sn$; Voigt-type bulk modulus B_V and Reuss-type bulk modulus B_R; Voigt-type shear modulus G_V and Reuss-type shear modulus G_R ; The data presented in parentheses are cited for comparison.

	C_{11} (GPa)	C_{22} (GPa)	C_{33} (GPa)	C_{12} (GPa)	C_{13} (GPa)	C_{23} (GPa)	C_{44} (GPa)	C_{55} (GPa)	C_{66} (GPa)	B_V (GPa)	B_R (GPa)	G_V (GPa)	G_R (GPa)
Cu	134.8 (169.1)[a]			109.5 (122.2)[a]			51.5 (75.4)[a]			117.9	117.9	35.9	23.1
Cu_3Sn	147.5 (154.6)[b]	165.0 (173.7)[b]	161.0 (148.2)[b]	82.9 (78.9)[b]	78.1 (76.5)[b]	79.4 (95.1)[b]	42.8 (50.2)[b]	47. 4 (44.2)[b]	45.5 (55.0)[b]	106.0	105.8	42.7	42.2
$(Cu_{0.9}Ni_{0.1})_3Sn$	156.8	201.5	244.6	88.3	103.5	124.6	46.7	53.8	45.3	137.3	128.4	48.2	47.4
$(Cu_{0.8}Ni_{0.2})_3Sn$	182.7	189.2	255.6	98.2	113.2	117.7	48.0	57.7	49.4	142.9	137.8	50.9	50.1
$(Cu_{0.7}Ni_{0.3})_3Sn$	194.8	200.9	268.5	104.7	116.7	117.7	51.7	58.5	50.4	149.2	145.0	53.8	53.0

a: the experimental elastic constants of Cu are cited from Ref.[26]

b: the calculated elastic constants of Cu_3Sn are cited from Ref.[27]

Table 2: Bulk modulus B; Shear modulus G; Young's Modulus E, Poisson ration υ; Universal anisotropy A^U; Ductility index B/G, The minimum Young's modulus, E_{min}, and corresponding orientation $[l_1,l_2,l_3]_{min}$,; The maximum Young's modulus, E_{max}, and corresponding orientation $[l_1,l_2,l_3]_{max}$, l_1, l_2, l_3 are the direction cosine of the orientation axis. The data presented in parentheses are cited for comparison.

	B (GPa)	G (GPa)	E (GPa)	υ	A^U	B/G	E_{min} (GPa)	$[l_1,l_2,l_3]_{min}$	E_{max} (GPa)	$[l_1,l_2,l_3]_{max}$
Cu	117.9 (140)[c]	29.5 (46.4)[c]	81.8 (112)[c]	0.384 (0.364)[c]	2.77	4.00	36.7	[1, 0, 0]	134.8	[0.5774, 0.5774, 0.5774]
Cu_3Sn	105.9	42.5	112.3	0.323	0.052	2.49	93.9	[1, 0, 0]	118.6	[0.5918, 0.5137, 0.6212]
$(Cu_{0.9}Ni_{0.1})_3Sn$	132.9	47.9	128.1	0.339	0.160	2.78	103.9	[1, 0, 0]	147.9	[0.2978, 0, 0.9546]
$(Cu_{0.8}Ni_{0.2})_3Sn$	140.4	50.5	135.21	0.339	0.121	2.78	116.8	[1, 0, 0]	161.8	[0, 0,1]
$(Cu_{0.7}Ni_{0.3})_3Sn$	147.1	53.4	142.9	0.338	0.107	2.76	124.9	[1, 0, 0]	177.8	[0, 0,1]

c: the experimental elastic modulii of Cu are cited from Ref.[28]

Table 3: The thickness of interface layer ***α***, tensile modulus $E_{tensile}$, ultimate tensile stress UTS, strain at UTS, work of adhesion W_{ad}, and interfacial toughness $K_{IC}^{interface}$ of $(Cu_xNi_{1-x})_3Sn$/Cu interfaces.

	α(m)	$E_{tensile}$(Pa)	UTS(GPa)	Strain at UTS	W_{ad} (J/m^2)	$K_{IC}^{interface}$ (MPa·m$^{0.5}$)
Cu_3Sn/Cu	6.96×10^{-10}	6.03×10^{10}	4.35	0.16	0.349	0.290
$(Cu_{0.9}Ni_{0.1})_3Sn$/Cu	6.96×10^{-10}	7.04×10^{10}	4.77	0.16	0.374	0.325
$(Cu_{0.8}Ni_{0.2})_3Sn$/Cu	6.96×10^{-10}	7.35×10^{10}	5.08	0.19	0.483	0.377
$(Cu_{0.7}Ni_{0.3})_3Sn$/Cu	6.96×10^{-10}	7.67×10^{10}	5.13	0.13	0.305	0.306

References

1. Kroupa, A.; Watson, A.; Mucklejohn, S.; Ipser, H.; Dinsdale, A.; Andersson, D., Chapter 5 -

Lead-Free Soldering: Environmentally Friendly Electronics. In *Green and Sustainable Manufacturing of Advanced Material*, Singh, M.; Ohji, T.; Asthana, R., Eds. Elsevier: Oxford, 2016; pp 101-134.

2. Li, S.; Wang, X.; Liu, Z.; Jiu, Y.; Zhang, S.; Geng, J.; Chen, X.; Wu, S.; He, P.; Long, W., *Journal of Materials Science: Materials in Electronics* **2020,** *31* (12), 9076-9090. doi:10.1007/s10854-020-03540-2

3. Mohd Nazeri, M. F.; Yahaya, M. Z.; Gursel, A.; Cheani, F.; Masri, M. N.; Mohamad, A. A., *Soldering & Surface Mount Technology* **2019,** *31* (1), 52-67. doi:10.1108/SSMT-05-2018-0013

4. Ramli, M. I. I.; Mohd Salleh, M. A. A.; Yasuda, H.; Chaiprapa, J.; Nogita, K., *Materials & Design* **2020,** *186*, 108281. doi:10.1016/j.matdes.2019.108281

5. Ma, H.; Kunwar, A.; Liu, Z.; Chen, J.; Wang, Y.; Huang, M.; Zhao, N.; Ma, H., *Journal of Materials Science: Materials in Electronics* **2018,** *29* (6), 4383-4390. doi:10.1007/s10854-017-8428-7

6. Wang, Z.; Zhang, Q. K.; Chen, Y. X.; Song, Z. L., *Journal of Materials Science: Materials in Electronics* **2019,** *30* (20), 18524-18538. doi:10.1007/s10854-019-02206-y

7. Le, W. K.; Ning, X.; Ke, C. B.; Zhou, M. B.; Zhang, X. P., *Journal of Materials Science: Materials in Electronics* **2019,** *30* (16), 15184-15197. doi:10.1007/s10854-019-01891-z

8. Liu, X.; He, S.; Nishikawa, H., *Scripta Materialia* **2016,** *110*, 101-104. doi:10.1016/j.scriptamat.2015.08.011

9. Zeng, G.; McDonald, S.; Nogita, K., *Microelectronics Reliability* **2012,** *52* (7), 1306-1322. doi:10.1016/j.microrel.2012.02.018

10. Michaelson, H. B., *Journal of Applied Physics* **1977,** *48* (11), 4729-4733. doi:10.1063/1.323539

11. Liu, J.-C.; Wang, Z.-H.; Xie, J.-Y.; Ma, J.-S.; Shi, Q.-Y.; Zhang, G.; Suganuma, K., *Corrosion Science* **2016,** *112*, 150-159. doi:10.1016/j.corsci.2016.07.004

12. El-Daly, A. A.; El-Taher, A. M.; Dalloul, T. R., *Materials & Design* **2014,** *55*, 309-318. doi:10.1016/j.matdes.2013.10.009

13. Wang, K.-K.; Gan, D.; Hsieh, K.-C., *Thin Solid Films* **2014,** *562*, 398-404. doi:10.1016/j.tsf.2014.05.003

14. Gonze, X.; Amadon, B.; Anglade, P.-M.; Beuken, J.-M.; Bottin, F.; Boulanger, P.; Bruneval, F.; Caliste, D.; Caracas, R.; Côté, M.; Deutsch, T.; Genovese, L.; Ghosez, P.; Giantomassi, M.; Goedecker, S.; Hamann, D. R.; Hermet, P.; Jollet, F.; Jomard, G.; Leroux, S.; Mancini, M.; Mazevet, S.; Oliveira, M. J. T.; Onida, G.; Pouillon, Y.; Rangel, T.; Rignanese, G.-M.; Sangalli, D.; Shaltaf, R.; Torrent, M.; Verstraete, M. J.; Zerah, G.; Zwanziger, J. W., *Computer Physics Communications* **2009,** *180*, 2582-2615. doi:10.1016/j.cpc.2009.07.007

15. Fuchs, M.; Scheffler, M., *Computer Physics Communications* **1999,** *119* (1), 67-98. doi:10.1016/S0010-4655(98)00201-X

16. Perdew, J. P.; Burke, K.; Ernzerhof, M., *Physical Review Letters* **1996,** *77* (18), 3865-3868. doi:10.1103/PhysRevLett.77.3865

17. Bellaiche, L.; Vanderbilt, D., *Physical Review B* **2000,** *61* (12), 7877-7882. doi:10.1103/PhysRevB.61.7877

18. Hua, G.; Li, D., *RSC Advances* **2015,** *5* (125), 103686-103694. doi:10.1039/c5ra22756a

19. Hua; Guomin; Li; Changsheng; Cheng; Xiaonong; Zhao; Xinluo; Feng; Quan, *Solid State Communications* **2018,** *269*, 102. doi:10.1016/j.ssc.2017.10.001

20. Hua, G.; Zhong, J.; Qi, Y.; Cheng, X., *Journal of the American Ceramic Society* **2018,** *101* (12), 5717-5731. doi:10.1111/jace.15862

21. Hua, G.; Chen, L.; Yang, J.; Qi, Y.; Dong, X.; Li, D.; Zhang, S.; Cheng, X., *Journal of Alloys and Compounds* **2019,** *803*, 379-393. doi:10.1016/j.jallcom.2019.06.228

22. Yu, H.; Vuorinen, V.; Kivilahti, J. K., *Journal of Electronic Materials* **2007,** *36* (2), 136-146. doi:10.1007/s11664-006-0028-x

23. Beckstein, O.; Klepeis, J. E.; Hart, G. L. W.; Pankratov, O., *Physical Review B* **2001,** *63* (13), 134112. doi:10.1103/PhysRevB.63.134112

24. Hill, R., *Proceedings of the Physical Society. Section A* **1952,** *65* (5), 349. doi: 10.1088/0370-1298/65/5/307

25. Wu, Z.-j.; Zhao, E.-j.; Xiang, H.-p.; Hao, X.-f.; Liu, X.-j.; Meng, J., *Physical Review B* **2007,** *76* (5), 054115. doi:10.1103/PhysRevB.76.054115

26. Ledbetter, H. M.; Naimon, E. R., *Journal of Physical and Chemical Reference Data* **1974,** *3* (4), 897-935. doi:10.1063/1.3253150

27. Pang, X. Y.; Wang, S. Q.; Zhang, L.; Liu, Z. Q.; Shang, J. K., *Journal of Alloys & Compounds* **2008,** *466* (1-2), 517-520. doi:10.1016/j.jallcom.2007.11.095

28. Committee, A. H., *ASM Handbook Vol. 2: Properties and Selection: Nonferrous Alloys and Special Purpose Materials 10 Ed.* ASM International: 1990.

29. Ranganathan, S. I.; Ostoja-Starzewski, M., *Physical Review Letters* **2008,** *101* (5), 055504. doi:10.1103/PhysRevLett.101.055504

30. Greaves, G. N.; Greer, A. L.; Lakes, R. S.; Rouxel, T., *Nature Materials* **2011,** *10* (11), 823-837. doi:10.1038/nmat3134

31. Pugh, S. F., *The London, Edinburgh, and Dublin Philosophical Magazine and Journal of Science* **1954,** *45* (367), 823-843. doi:10.1080/14786440808520496

32. Nye, J. F., *Physical Properties of Crystals: Their Representation by Tensors and Matrices*. Clarencon Press: Oxford, 1985.

33. Ohring, M., *The Material Science of Thin Films*. Academic Press: San Diego, 1992.

34. Momma, K.; Izumi, F., *Journal of Applied Crystallography* **2011,** *44* (6), 1272-1276. doi:10.1107/S0021889811038970